Combustion and Flame 242 (2022) 112183

Contents lists available at ScienceDirect

Combustion and Flame

journal homepage: www.elsevier.com/locate/combustflame

Measurement and scaling of turbulent burning velocity of ammonia/methane/air propagating spherical flames at elevated pressure

Hongchao Dai, Jinhua Wang*, Xiao Cai, Shouguo Su, Haoran Zhao, Zuohua Huang

State Key Laboratory of Multiphase Flow in Power Engineering, Xi'an Jiaotong University, Xi'an 710049, China

ARTICLE INFO

Article history:
Received 15 November 2021
Revised 29 April 2022
Accepted 30 April 2022

Keywords:
Turbulent burning velocity
Turbulent burning velocity correlation
Integral length scale effect
Propagating spherical flame
Ammonia

ABSTRACT

This study reports the accurate laminar burning velocity, turbulent burning velocity and its correlations of ammonia/methane/air propagating spherical flames. The experiments were carried out on a medium-scale, fan-stirred cylindrical combustion chamber with ammonia molar content varying from 20% to 60% and the initial pressure up to 3 bar. The turbulent burning velocity decreases with the ammonia content due to the weakening effect of the laminar burning velocity under all turbulence intensities and pressures studied. Since the weakening of flame chemistry is dominated by the enhancement of turbulence eddies, the normalized turbulent burning velocity increases with the ammonia content. The turbulent expanding flame of ammonia/methane/air is self-similar under different ammonia content. This self-similar propagation follows the one-half power-law correlation between the normalized turbulent burning velocity, S_T/S_L, and the turbulent flame Reynolds number, which is quantitatively consistent with that of unity Lewis number methane/air flames (Chaudhuri 2012). The pressure dependence of turbulent burning velocity can be represented roughly as a 0.4 power law of S_T/S_L and $(u'/S_L)(P/P_0)$. However, there is a quantitative gap between the pre-exponential factor of the present experimental data and the literature data based on this correlation, which could attribute to the difference in the turbulence eddy scales of different experimental apparatus. The integral length scale characterized the largest turbulence eddies is introduced to consider the turbulent length scale effect. A modified general correlation $S_T/S_L \sim (L_I/L_0)^{0.5}[(u'/S_L)(P/P_0)]^{0.41}$ with the consideration of the integral length scale effect is obtained, which is able to predict a variety of spherical flame data regardless of temperatures, pressures, and fuel types. In addition, it is verified that turbulent burning velocity of ammonia flame could be expressed by the correlation of Karlovitz and Damköhler numbers: $S_T/S_L \sim Ka \cdot Da = Re_{T,\ flow}{}^{0.5}$. It can be seen that ammonia has similar turbulent combustion characteristics as hydrocarbon fuel. These findings indicate that it is feasible to simulate and optimize ammonia combustors utilizing previous turbulent burning velocity correlations based on hydrocarbon fuel.

1. Introduction

Ammonia is recognized as a promising hydrogen carrier and carbon-free fuel due to its property that can be synthesized from renewable energy, its low liquefaction, transportation and storage costs as well as high hydrogen density. However, its practical application is hindered by the low laminar burning velocity, high NO_X emission, large ignition energy, and narrow stability range [1]. Co-firing ammonia with hydrogen [2–5], methane [6–8], syngas [9], and DME [10,11] is considered as a possible solution to overcome these obstacles.

Recently, ammonia/methane cofiring has been conducted in industrial burners [12,13], which proves that ammonia has great potential to be burned with methane. Studying the fundamentals of ammonia/methane flame is essential for the development of ammonia combustion technology [14]. Laminar burning velocity is one of the most important fundamental parameters to characterize the combustion behavior of combustible mixture, and it is also a key parameter for some premixed flame phenomena, such as propagation, extinction, flashback, blow-off and turbulent combustion [15]. Extensive fundamental experimental and kinetic modeling studies have been conducted on the laminar combustion properties of blending methane into ammonia in different devices [6,16-23]. However, the turbulent burning velocity of ammonia, as a characterization of the operating state of the practical combustors, has not been widely investigated. Ichikawa et al. [7] measured the tur-

* Corresponding author.
E-mail address: jinhuawang@xjtu.edu.cn (J. Wang).

https://doi.org/10.1016/j.combustflame.2022.112183
0010-2180/

bulent burning velocity of methane/ammonia/air mixtures using nozzle burners at 0.5 MPa and 298 K with an ammonia molar content in the range of 0–39%. Considering the weak combustion intensity of ammonia, Hashimoto et al. [24,25] successively focus on the turbulent flame propagation limits of ammonia/air and ammonia/methane/air in a constant volume vessel. Subsequently, Xia et al. [26] used the same constant volume vessel to obtain the turbulent burning velocity of ammonia under oxygen-rich conditions and suggested that turbulence intensity and diffusional-thermal instability may play an important role in the turbulent burning velocity. In addition, based on the measurement of turbulent burning velocity, Xia and Hadi et al. [27, 28] explained the basic mechanism of the effect of ammonia oxidizer equivalence ratio and fuel ratio on the turbulent burning velocity of ammonia/pulverized coal co-combustion. Lhuillier et al. [29] respectively studied the effects of blending methane or hydrogen with volume content ranging from 0 to 15% on the turbulent burning velocity of ammonia at 445 K and 0.54 MPa, and suggested that these data have a good correlation with Karlovitz number and Damköhler number. Recently, Wang et al. [30] studied the oxygen-rich turbulent combustion of ammonia with wide oxygen contents. They found that ammonia/oxygen/nitrogen flame has self-similar propagation nature, which can be represented by the classical turbulent burning velocity model. Although previous studies have provided the necessary information and understanding of the ammonia turbulent flame, there is still a lack of turbulence experimental research and data for ammonia with a wide range of methane content, pressure and turbulence intensity, which is essential to improve a premixed type ammonia combustor and develop turbulent combustion model [31].

Seeking a possible unified scaling description of turbulent burning velocity independent of the flame geometries, experimental conditions and fuels is not only conducive to basic understanding, but also can be used as a quantity of critical importance for the LES sub-grid model to simulate combustion processes [32–34]. In 1940, Damköhler [35] advanced the fundamental concept on turbulent flames, suggesting that the large-scale turbulence increases the flame surface area and causes the increase of turbulent burning velocity, while the small-scale turbulence enhances the mass and thermal diffusivity in the flame preheat zone by changing the molecular transport between the reaction zone and the preheated gas. For the small-scale turbulence corresponding to the thin reaction zone, Damköhler proposed $\frac{S_T}{S_L} \sim (\frac{u'L_I}{\nu})^{\frac{1}{2}}$, where u', L_I, ν, represent the turbulence intensity, integral length scale, and kinematic viscosity of the mixture, respectively. Kobayashi et al. [36,37] measured turbulent burning velocity data of methane/air up to 3 MPa using a turbulent Bunsen burner to clarify the effect of high pressure on flame-turbulence interaction. Then, Kobayashi et al. [36,37] reported a general correlation for the normalized turbulent burning velocity of methane flames considering the influence of pressure, $\frac{S_T}{S_L} \sim (\frac{u'}{S_L}\frac{P}{P_0})^{0.38}$. Based on the turbulent expanding flame experimental of unity Lewis number methane/air flame with ϕ = 0.9, Chaudhuri et al. [32] found that the turbulent flame speed always accelerates during the propagation process. Considering the unique self-similar accelerated propagation of the turbulent expanding flame, Chaudhuri et al. [32] proposed to replace the turbulent integral scale L_I to the turbulent flame radius $\langle r \rangle$, and develop a general correlation $\frac{S_T}{S_L} \sim (\frac{u'}{S_L}\frac{\langle r \rangle}{\delta})^{\frac{1}{2}} = (Re_{T,\ flame})^{\frac{1}{2}}$ for turbulent propagating flames, where $Re_{T,\ flame}$ is the turbulent flame Reynolds number. Shy and co-workers [31,38,39] obtained the S_T data of methane, hydrogen, propane flames under high temperatures and high pressures using the cruciform bomb, and verified the correlations of Chaudhuri [32] and Kobayashi [36,37], and proposed that the S_T correlation based on Damköhler number, *Da*. It is worth noting that some researchers [33,40-46] have also studied the S_T correlation with *Le* not equal to unity to illustrate the effects of molecular diffusion, which is almost inseparable from the theoretical basis of the above model. Since the combustion intensity of ammonia is much weaker than that of conventional hydrocarbon fuels, whether these correlations developed based on hydrocarbon fuels are applicable to ammonia fuel is still a question.

In view of the above considerations, we have two major objectives in the present work. Firstly, we reported the turbulent burning velocity of ammonia/methane/air mixtures with a wide range of ammonia volume content at elevated pressure using a medium-scale fan-stirred cylindrical chamber. Secondly, considering the similar molecular diffusion characteristics of ammonia and methane, we verified the applicability of the classical turbulence correlations by using S_T data under different ammonia content measured in this work and pure methane S_T data from the literature. In addition, we also found the inconsistency of the turbulence correlations, which attributes to the inadequate consideration of turbulence length scale effects. Therefore, based on the present experimental data, we obtained a modified general correlation with the integral length scale consideration. This correlation showed a good agreement with the present experimental data and the methane data of unity Lewis number at different temperatures and pressures.

2. Experimental and numerical methods

2.1. Experimental setup

The experiment was carried out in a medium-scale, cylindrical type, spark ignition chamber with four orthogonally arranged fans, an inner diameter of 303 mm, an inner length of 307 mm, and a volume of 22.6 L, as shown in Fig. 1. The detailed description of the experimental device has been introduced in Cai et al. [47] and Zhao et al. [48]. In brief, two quartz glass windows with 150 mm diameter and 60 mm thickness are installed on opposite sides of the chamber for flame visualization. The quasi-isotropic turbulence field in the window area is generated by the rotation of four identical orthogonally arranged fans inside the chamber. The fan diameter is 114 mm with five blades, and the central experimental diameter of about 240 mm can be obtained. Four independent motor speed controllers drive the motors and fans to rotate at a given speed.

Based on partial pressure law, the partial pressure of each component is quantified by a piezoelectric pressure sensor (Kistler 6125C) with the accuracy of 0.04% in full scale. The fuel, oxygen and nitrogen are successively induced into the chamber that has been vacuumed. The purities of ammonia, methane, oxygen and nitrogen stored in cylinder gas are all 99.999%. Air was prepared with O_2 and N_2 in a mole ratio of 21/79. For laminar cases, the combustible gases are fully mixed after three minutes and centrally ignited by the spark ignition, while for turbulent cases, the fans are driven at the set fan speed before igniting the mixtures, and the fans are continuous running in the whole flame propagation event. A pair of 1.0 mm tungsten electrodes arranged in line with a 1.5 mm gap is selected for spark ignition. Each ignition is set to a 1 ms discharge time with the average ignition energy of ~150 mJ. The centrally-ignited flame propagation images are recorded by a shadow photography system through a Phantom v611 camera operating at 10,000 fps with the image resolution of 752 × 752 pixels and the magnification ratio of 0.23 mm/pixel. The propagating flame front is track from the images using a MATLAB algorithm for post-processing. In addition, each laminar case is repeated 2–3 times, and the turbulent case is repeated 4–5 times to reduce random errors. Uncertainties in experiments are mainly introduced by experimental setting deviation related to T_u, P, ϕ and u', statistical errors related to repeatability, radiation-induced

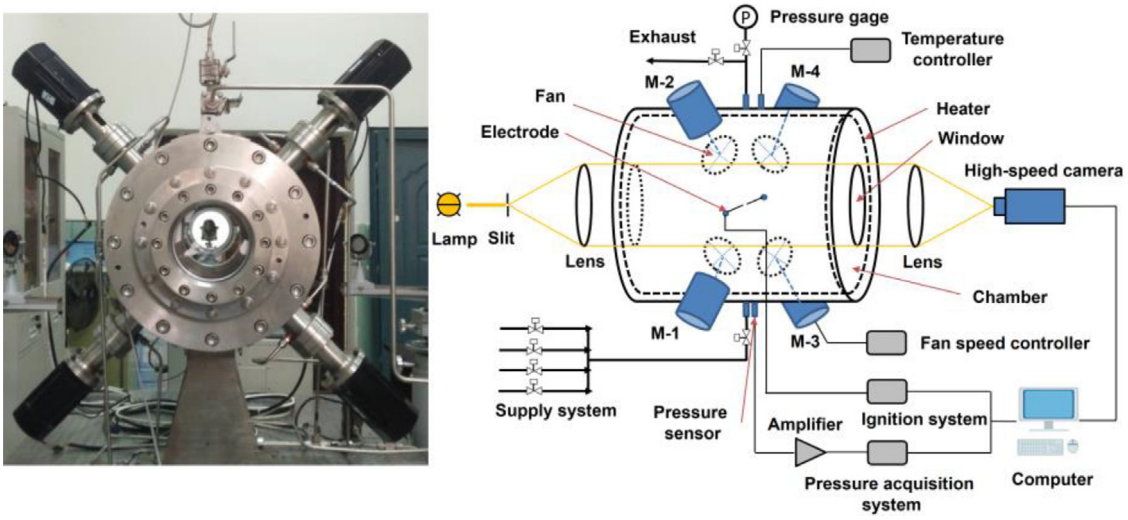

Fig. 1. Image and schematic of experimental setup.

uncertainty, etc. The total bias uncertainty and statistical errors have been evaluated using the method proposed by Moffat et al. [49] with a 95% confidence level. The overall uncertainty of the S_L is ± 0.9–2.6 cm/s, which mainly comes from the radiation-induced uncertainty and statistical errors. The turbulence experimental uncertainty is estimated to be ±3.2–9.6 cm/s, mainly depending on random errors. The detailed uncertainty analysis process can be found in the *Supplementary Material*.

The cold turbulence flow field inside the fan-stirred turbulent combustion chamber was previously calibrated by a 2D particle image velocimetry (PIV) with fan rotation speeds from 500 to 2000 rpm and pressures ranging from 0.05 to 0.5 MPa [47]. The PIV system and optical configuration are shown in Fig. S1. The important parameters to characterize the turbulent flow are the turbulence intensity determined by the rms turbulent fluctuation velocity and integral length scale which captures the mean size of large eddies. It was found that the turbulence intensity, u', is proportional to the fan speed, n, as shown in Eq. (1).

$$u' = 0.00181 \times n \ (\mathrm{m/s}) \tag{1}$$

The longitudinal integral length scale, L_I, increases non-linearly with the fan speed, n, which is in accordance with $L_I = 16.44(1 - 0.998^n)$ (mm).

2.2. Experimental conditions and data processing methods

The experiments were carried out at initial temperature of 298 K and initial pressures of 1 to 3 bar. X_{NH3} represents the mole fraction of ammonia in the binary fuel, where $X_{NH3} = mol(NH_3)/[mol(NH_3) + mol(CH_4)]$. The X_{NH3} was conducted from 0 to 60%. Previous findings showed that a low level of NO_x emissions could be obtained when the ammonia volume content in the mixed fuel does not exceed 60% [50]. In laminar cases, ammonia/methane/air mixtures were performed with the equivalence ratio varying from 0.8 to 1.3. The experimental conditions and properties of laminar flames are listed in Table 1. The turbulent flame was conducted under the stoichiometric condition since the Lewis number, *Le*, of the ammonia/methane/air mixture is close to unity at different equivalence ratios. The fan rotation speeds are varied from 0 to 1500 rpm, and the corresponding maximum turbulence intensity is 2.72 m/s. The experimental conditions and properties of turbulent flame are summarized in Table 2.

The equivalent flame radius of the flame is obtained using the enclosed area of the flame front, $\langle r \rangle = (A_f/\pi)^{0.5}$. To eliminate the influence of ignition and chamber confinement, the flame radius is selected within the range of 15 mm to 45 mm based on the analysis result [52]. The laminar flame propagation speed S_b is calculated by $d\langle r \rangle/dt$. The unstretched laminar flame propagation speed, $S_b{}^0$ is estimated by the non-linear extrapolation method proposed by Kelley et al. [51] as $(\frac{S_b}{S_b^0})^2 ln(\frac{S_b}{S_b^0})^2 = -2\frac{L_b K}{S_b^0}$ with Markstein length, L_b, and the flame stretch rate, K, calculated from $\frac{2}{r}\frac{d\langle r \rangle}{dt}$. Then, the laminar burning velocity can be obtained as $S_L = S_b^0/\sigma$, where σ is the ratio of unburned to burned gas density. The detailed S_L determination process can be found in the *Supplementary Material*. The flame fronts appear obvious irregular wrinkles under turbulent conditions. Bradley et al. [53] suggested that the turbulent flame radius of the schlieren images cor-

Table 1
Laminar flame conditions and properties of ammonia/methane/air mixtures. The initial temperature is 298 K.

X_{NH3}	P (bar)	ϕ	Σ	T_{ad} (K)	S_L (m/s)[a]	δ (mm)[b]	Le_{eff}[c]
0.2	1	0.8	6.69	1982	0.188	0.68	1.03
		0.9	7.16	2118	0.239	0.60	1.03
		1.0	7.51	2210	0.273	0.57	1.06
		1.1	7.54	2190	0.266	0.57	1.09
		1.2	7.41	2116	0.239	0.64	1.09
		1.3	7.26	2038	0.163	0.88	1.09
0.4	1	0.8	6.67	1965	0.146	0.84	1.03
		0.9	7.14	2099	0.190	0.73	1.03
		1.0	7.49	2192	0.214	0.70	1.06
		1.1	7.51	2167	0.209	0.71	1.09
		1.2	7.38	2091	0.181	0.85	1.09
		1.3	7.23	2014	0.117	1.16	1.09
0.6	1	0.8	6.64	1942	0.116	1.12	1.03
		0.9	7.11	2073	0.147	0.97	1.03
		1.0	7.47	2167	0.160	0.92	1.06
		1.1	7.47	2135	0.157	0.95	1.09
		1.2	7.33	2059	0.126	1.18	1.09
		1.3	7.18	1984	0.090	1.45	1.09
0	3	1	7.58	2246	0.237	0.20	1.06
0.1		1	7.57	2239	0.217	0.24	1.06
0.2		1	7.57	2231	0.185	0.26	1.06
0.3		1	7.56	2222	0.160	0.30	1.06
0.4		1	7.55	2211	0.142	0.33	1.06
0.5		1	7.53	2198	0.117	0.38	1.06
0.6		1	7.51	2183	0.103	0.44	1.06

[a] Laminar burning velocity is measured with a non-linear extrapolation method [51].
[b] The laminar flame thickness, $\delta = (T_{ad} - T_u)/(dT/dx)_{max}$.
[c] The effective Lewis number, $Le_{eff} = X_{NH3}Le_{NH3} + X_{CH4}Le_{CH4}$.

Table 2
Turbulent flame conditions and properties of stoichiometric ammonia/methane/air mixtures. The initial temperature is 298 K.

X_{NH3}[a]	P (bar)	u' (m/s)[b]	L_I (mm)[b]	u'/S_L	S_T (cm/s)[c]	$S_{T,c\ =\ 0.5}$ (cm/s)[d]	Ka[e]	Da[f]	$Re_{T,\ flow}$[g]
0.2	1	0.91	10.4	3.31	42.44	83.18	1.40	5.55	61
	1	1.36	12.8	4.96	52.10	102.12	2.33	4.54	112
	1	1.81	14.2	6.62	57.86	113.41	3.40	3.79	166
	1	2.72	15.6	9.93	68.06	133.40	5.96	2.78	274
	3	0.91	10.4	4.88	47.85	93.79	1.72	8.05	192
	3	1.81	14.2	9.77	71.44	140.02	4.16	5.51	525
	3	2.72	15.6	14.65	82.91	162.51	7.29	4.03	865
0.4	1	0.91	10.4	4.24	35.90	70.36	2.26	3.53	63
	1	1.36	12.8	6.36	42.46	83.22	3.74	2.89	117
	1	1.81	14.2	8.48	48.96	95.97	5.46	2.41	173
	1	2.72	15.6	12.71	59.51	116.63	9.56	1.77	286
	3	0.91	10.4	6.36	39.00	76.43	2.87	4.90	198
	3	1.81	14.2	12.71	53.52	104.90	6.95	3.35	541
	3	2.72	15.6	19.07	69.45	136.13	12.18	2.45	892
0.6	1	0.91	10.4	5.80	27.25	53.41	4.14	1.96	66
	1	1.36	12.8	8.70	32.70	64.09	6.86	1.61	122
	1	1.81	14.2	11.60	37.43	73.35	10.01	1.34	181
	1	2.72	15.6	17.39	42.41	83.13	17.59	0.98	296
	3	0.91	10.4	8.80	33.28	65.23	5.34	2.72	210
	3	1.81	14.2	17.60	45.33	88.84	12.92	1.86	575
	3	2.72	15.6	26.40	56.72	111.18	22.64	1.36	948

[a] The mole fraction of NH_3 to binary fuel of NH_3 and CH_4.
[b] $u' = 0.00181 \times n$ (m/s) and $L_I = 16.44(1 - 0.998^n)$ (mm).
[c] The turbulent burning velocity obtained by shadow image corresponding to the mean progress variable $\langle c \rangle \approx 0.1$.
[d] The turbulent burning velocity corresponding to the mean progress variable $\langle c \rangle \approx 0.5$, $S_{T,\ c=0.5} = (\langle r \rangle_{c=0.1}/\langle r \rangle_{c=0.5})^2 S_T$ and $\langle r \rangle_{c=0.1}/\langle r \rangle_{c=0.5} \approx 1.4$.
[e] The Kalovitz number, $Ka = (u'/S_L)^{\frac{3}{2}}(L_I/\delta)^{-\frac{1}{2}}$.
[f] The Damköhler number, $Da = (u'/S_L)^{-1}(L_I/\delta)$.
[g] The turbulent Reynolds number, $Re_{T,flow} = (u'/S_L)/(L_I/\delta)$.

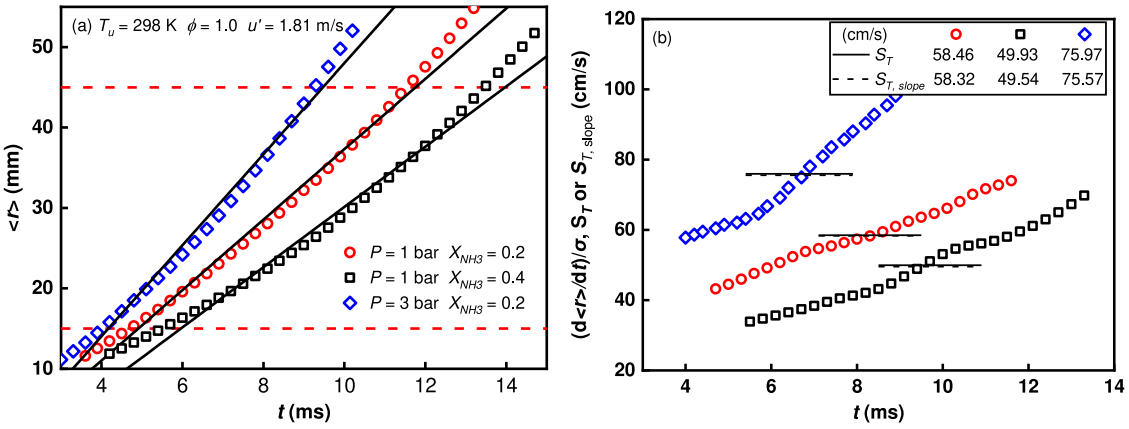

Fig. 2. (a) The typical flame radius versus time measured at different pressures and X_{NH3}. (b) Three turbulent burning velocities ($(d\langle r \rangle/dt)/\sigma$, S_T and $S_{T,slope}$) are plotted against time.

responds to the mean progress variable $\langle c \rangle \approx 0.1$. Further, the flame fronts captured by the shadow method and the schlieren method can be considered to be consistent, as shown in the *Supplementary Material*. The turbulent flame propagation speed is determined by the quotient of differential of the flame radius versus time $d\langle r \rangle/dt$ and density ratio σ. And the global turbulent burning velocity, S_T, is determined as the average value of the turbulent flame propagation speed within a radius ranging from 15 mm to 45 mm.

Figure 2(a) shows the flame radii versus time under three typical turbulent conditions and whose best linear-fit line with $\langle r \rangle$ ranging from 15 to 45 mm. Shy et al. [38] determined the slope of the best linear-fit line and then divided by the density ratio as the global turbulent burning velocity, $S_{T,slope}$. In Fig. 2(b), the flame propagation speed and the global turbulent burning velocities with two kinds of definition are compared corresponding to $\langle r \rangle$ = 15–45 mm. The turbulent flame propagation speed $(d\langle r \rangle/dt)/\sigma$ increases continuously and represents the accelerative propagation of the spherical expanding flame. The global turbulent burning velocities obtained from two kinds of definition (S_T and $S_{T,slope}$) are almost the same under different conditions. And the definition of averaged turbulent flame propagation will be used to represent the global turbulent burning velocity, S_T, in following.

The fundamental flame parameters, such as density ratio, σ, adiabatic flame temperature, T_{ad}, and S_L are calculated by using the Equilibrium and 1D freely propagating flame module of CHEMKIN-Pro with the chemical kinetic model of Okafor et al. [6]. The flame thickness, δ, is estimated as $\delta = (T_{ad} - T_u)/(dT/dx)_{max}$, where T_u is the initial temperature and $(dT/dx)_{max}$ is the maximum temperature gradient [54]. The fuel Lewis number is calculated by weighting the Lewis numbers of ammonia and methane according to the volume fraction [55].

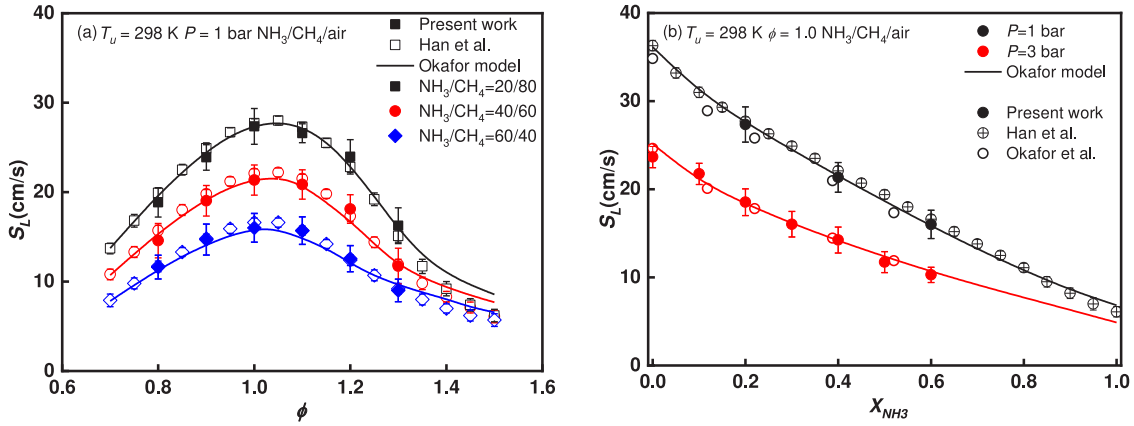

Fig. 3. Experimental and numerical laminar burning velocity of ammonia/methane/air at (a) different ϕ and (b) various X_{NH3}. The data from Okafor et al. [5] and Han et al. [19] are also shown.

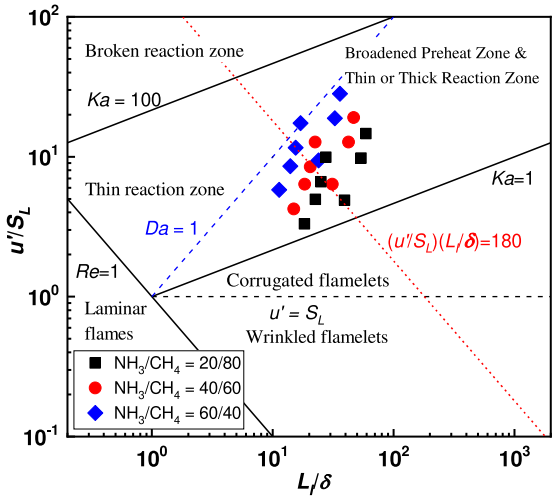

Fig. 4. Experimental conditions on the turbulent combustion regime diagram.

3. Results and discussions

3.1. Laminar burning velocity and turbulent combustion diagram

Figure 3(a) shows the comparison between the measured and simulated S_L of ammonia/methane/air with X_{NH3} ranging from 0.2 to 0.6. It is obvious that X_{NH3} has a significant influence on S_L for all equivalence ratios. Experimental and numerical results show that the maximum S_L are presented in a slightly fuel-rich side at about $\phi \approx 1.05$ for different X_{NH3}. It is observed that the numerical results are in good agreement with the experimental values for $\phi < 1.3$ but overestimate the S_L for over-rich flames ($\phi > 1.3$). Figure 3(b) shows the S_L of stoichiometric ammonia/methane/air flames as a function of X_{NH3}. The experimental values of S_L are compared with previous experimental data [6,20] and numerical results calculated with the mechanism of Okafor et al. [6]. The experimental values are in good agreement with the S_L measured using a heat flux burner by Han et al. [20] and a combustion bomb by Okafor et al. [6], which proves the reliability of the present experimental data. It can be seen that the S_L approximately decreases linearly with the increase of X_{NH3}. The oxidation of NH_3 and CH_4 can likely be understood as a process of parallel oxidation of independent fuels [20]. As the pressure increases, the S_L greatly decreases, and the Okafor Mech [9] could accurately predict the S_L under different pressures.

Figure 4 plots the experimental conditions on the Borghi–Peters' diagram [56]. All of the experimental conditions are distributed in the TRZ regime. In this regime, the flame surface is severely deformed, and the small-scale structure develops on the flame front. The turbulent Karlovitz number, $Ka > 1$, and the chemical time scale is greater than the turbulent eddy lifetimes, which means the small-scale eddies might enter the flame preheat zone and broaden the layer of preheat zone, while the reaction zone will keep thin. However, recent studies have found that preheat zone broadening does not necessarily occur in the TRZ and even in the Broken reaction zone proposed by Peters [56]. Skiba et al. [57] believes that the preheat zone becomes broadened when the turbulent diffusivity sufficiently exceeds the molecular diffusivity within the preheat layer by a factor of 180. This boundary line of $(u'/S_L)(L_I/\delta) = 180$ is plotted in Fig. 4, and it is found that half of the cases exceed this boundary. Recently, Gülder et al. [58] and Mohammadnejad et al. [59] found that both the preheat and reaction zones may thicken beyond this boundary. It is unclear whether the above boundary can be used for spherical flames. Ahmed et al. [60] experimental determined the ratio of turbulent burning rate enhancement to the flame surface area enhancement for spherical flames. However, quantitative studies of flame structure are still required to demonstrate whether the thickening phenomenon occurs in spherical flames.

3.2. Turbulent flame morphology and turbulent burning velocity

Figure 5 shows the typical flame images of ammonia/methane/air under different turbulence conditions. The *Le* is near unity for all conditions, thus the flame propagation is not affected by the diffusional-thermal instability. No hydrodynamic cells are observed on the flame front for the laminar flames, indicating the turbulent flames propagating without effects of hydrodynamic instability. In addition, the flame propagation is significantly enhanced by the imposed turbulence, thus the buoyancy effect is negligible. Therefore, the stoichiometric turbulent propagating flame is the result of the interaction between turbulence and flame chemistry, and is not affected by flame cellular instability.

As the X_{NH3} increases, the flame surface becomes more wrinkled at the same u', however, the time required for the flame front to expand to a 35 mm radius increases. This could be the result of lower S_L for ammonia enriched mixture, and it reveals that flame chemistry plays a dominant role in present case. As the u' increases, finer wrinkles appear on the flame front, and the irregularities of the flamelet increase due to the reduction of Kolmogorov scale. When u' reaches 2.72 m/s, flames with $X_{NH3} = 0.4$ will be

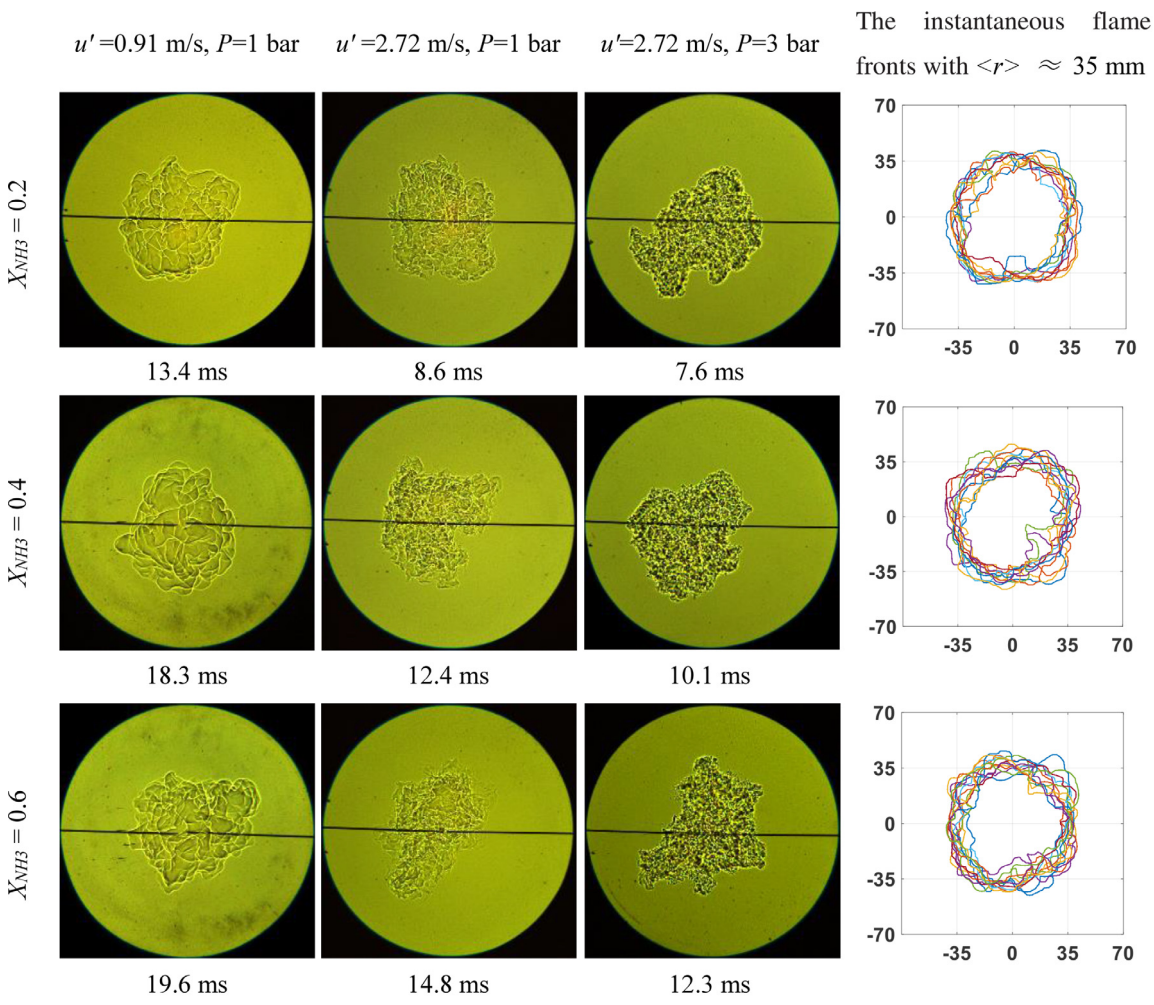

(a) Flame morphology under different ammonia molar contents, pressures and turbulence intensities. The <r> ≈ 35 mm for all images.

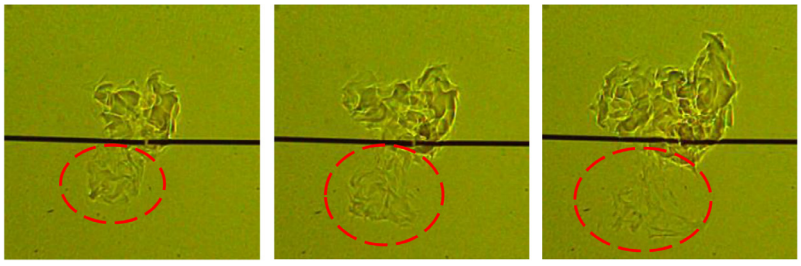

(b) Local extinction at X_{NH3} = 0.6, u' = 2.72 m/s and P = 1 bar. The time interval of image is 2.0 ms.

Fig. 5. Flame morphology of ammonia/methane/air mixtures under different turbulent conditions. (a) Flame morphology under different ammonia molar contents, pressures and turbulence intensities. The $\langle r \rangle \approx 35$ mm for all images. (b) Local extinction at $X_{NH3} = 0.6$, $u' = 2.72$ m/s and $P = 1$ bar. The time interval of image is 2.0 ms.

wrinkled, which is mainly due to the increase of the turbulence scale spectrum, and the eddies larger than the flame surface makes the flame convective. And local extinction appears at the initial stage of flame propagation at $X_{NH3} = 0.6$. Wu et al. [61] also found this phenomenon in n-octane/air turbulent flames and suggested that non-equidiffusion could suppress and promote local extinction for $Le < 1$ and $Le > 1$ cases, respectively. This also makes it difficult to define the boundary of the flame surface. When the pressure increases, the local extinction still appears under the same X_{NH3} and u'. The boundary of flame surface becomes sharper at elevated pressure since the flame becomes thinner and the flame surface density increases.

Figure 6(a) shows the S_T as a function of u' at different P and X_{NH3}. As expected, the smaller the X_{NH3}, the faster turbulent flame propagation due to the larger S_L. For all conditions, S_T increases quickly with u' in moderate turbulence, and it bends in intense

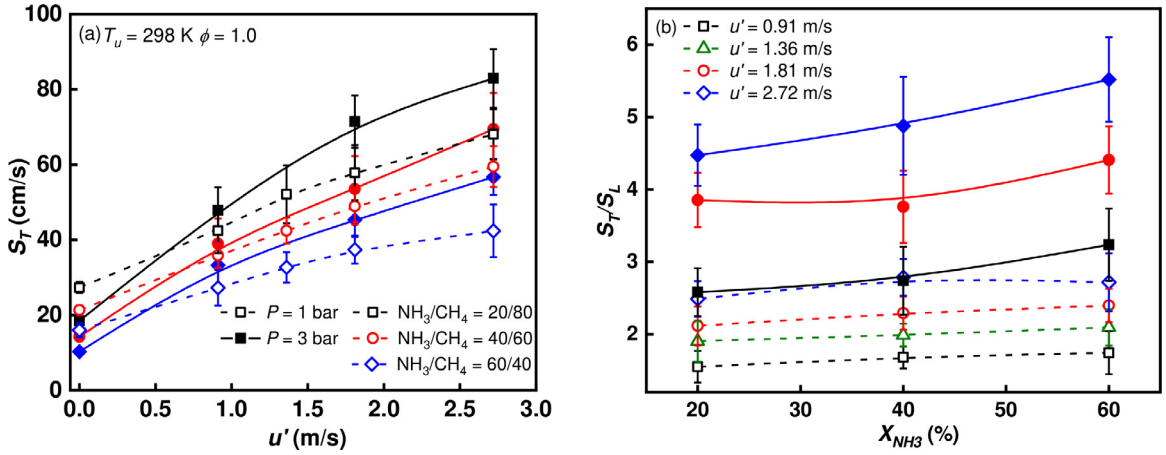

Fig. 6. The effects of P and X_{NH3} on (a) S_T and (b) S_T/S_L with $\phi = 1.0$. The hollow symbols show the experimental data under the pressure of 1 bar, while the solid symbols show that under the pressure of 3 bar.

turbulence. When u' exceeds a certain value, the S_T might eventually reach a peak value and will further decrease with the occurrence of significant local extinction. Although the peak of S_T is not reached in the present experiment, the bending effect is observed at different pressures as shown in Fig. 6(a). Mohammadnejad et al. [59] showed the bending behavior observed for other flame geometries also related to flame quenching/extinctions. Larger data dispersion can be observed under high u', because the flame is highly deformed in intense turbulence. The scale range of the turbulent eddies increases with u', which causes the non-uniformity influence of the turbulence eddies on the wrinkle of flame surface. Contrary to S_L, the S_T will further increase at elevated pressure. Such an increase in S_T is attributed to the additional flame front area, which is caused by the effect of the increase in the turbulent flow Reynolds number and decrease in the Kolmogorov scale under elevated pressure due to the reduced fluid viscosity [62].

Figure 6(b) shows the normalized turbulent burning velocity, S_T/S_L, as a function of the X_{NH3} at different pressures and u'. It can be seen that the S_T/S_L shows an overall increasing trend with the X_{NH3} at the same u'. The increase in ammonia content leads to a significant weakening of the flame chemistry, which exceeds the enhancement of turbulence eddies. Meanwhile, the increase of X_{NH3} is accompanied by the increase of Ka, indicating that the stretching influence of the turbulence vortex is strengthened. The increase in pressure can significantly enhance the effect of changes in the X_{NH3} on S_T/S_L. This illustrates that mixtures with high X_{NH3} and pressure are more susceptible to turbulence, which is mainly attributed to the increases in turbulence disturbance due to the higher Ka.

3.3. Possible general correlation of turbulent burning velocity

Chaudhuri et al. [32] proposed a power-law correlation as $(d\langle r\rangle/dt)(1/\sigma S_L) = 0.102 Re_{T,\ flame}{}^{0.54}$ to indicate the self-similar propagation of spherical flames based on the unity Le methane/air mixtures. This correlation has been verified by a series of hydrocarbon fuels [61], wide pressure range [39], and various turbulence intensities [47]. To verify the applicability of this correlation for unity Le ammonia/methane/air, variations of the normalized flame propagation speed with the turbulent flame Reynolds number under different P and u' at $\phi = 1.0$ are plotted in Fig. 7 . All the data in Fig. 7(a) with $X_{NH3} = 0.2$ can be collapsed to a single power-law correlation curve, $\frac{d\langle r\rangle/dt}{\sigma S_L} = 0.108 Re_{T,\ flame}{}^{0.51}$. The self-similar propagation is also observed in the mixtures with different X_{NH3} and P. This result represents the self-similar nature of propagating spherical flames regardless of fuel type, initial pressure, and turbulence intensity. Furthermore, all the data with different X_{NH3}, P, and u' collapse into a line through a power law correlation,

$$\frac{d\langle r\rangle/dt}{\sigma S_L} = 0.105 Re_{T,\ flame}{}^{0.53} \tag{2}$$

The difference of the pre-exponent factor and the power exponent between Eq. (5) and Chaudhuri's correlation is within 3%. This demonstrates that the correlation between normalized turbulent flame propagation speed and turbulent Reynolds number is also applicable to ammonia-containing fuels.

Figure 8 shows the S_T/S_L with different P and X_{NH3} as a function of the relative turbulence intensity, u'/S_L. It is found that under the same pressure, S_T/S_L has a similar variation behavior with u'/S_L for any X_{NH3}, indicating the strong pressure dependence of S_T/S_L. Kobayashi et al. [36,37] measured the S_T of methane/air Bunsen-type flames mixture with $\phi = 0.9$ ($Le \approx 1.0$), and found the same phenomenon, so they proposed the general correlation for turbulent burning velocity,

$$\frac{S_T}{S_L} = C\left(\frac{u'}{S_L}\frac{P}{P_0}\right)^{0.38} \tag{3}$$

where $P_0 = 1$ atm and $C = 5.04$ and 2.90 for the mean process variable $\langle c\rangle \approx 0.1$ and 0.5, respectively.

The turbulent burning velocity corresponding to $\langle c\rangle \approx 0.5$ of present work can be determined according to the progress variable conversion factor [53] by $S_{T,\ c=0.5} = (\langle r\rangle_{c=0.1}/\langle r\rangle_{c=0.5})^2 S_T$, where $\langle r\rangle_{c=0.1}/\langle r\rangle_{c=0.5} \approx 1.4$. Furthermore, Chaudhuri et al. [32] considered the effects of gas expansion and proposed to calculate the $S_{T,c=0.5}$ by $S_{T,\ c=0.5} = (2\sigma/(\sigma+1))\ (\langle r\rangle_{c=0.1}/\langle r\rangle_{c=0.5})^2 S_T$. Note that two conversion methods exist a difference of $2\sigma/(\sigma+1)$. Recently, Jiang et al. [39] and Wang et al. [30] respectively measured the S_T of methane/air mixture and ammonia/oxygen/nitrogen mixture using the spherical expanding flame, but using different conversion methods from $S_{T,\ c=0.1}$ to $S_{T,\ c=0.5}$. Jiang et al. [39] determined that $S_{T,\ c=0.5}$ by the former method mentioned above without considering the effects of gas expansion, while Wang et al. [30] used another method. Unexpectedly, the $S_{T,\ c=0.5}$ data of Jiang et al. [37] and Wang et al. [30] all verified the Kobayashi correlation [36] well, indicating the correlation proposed by Kobayashi et al. [36,37] may not be quantitatively unified for spherical flames.

As shown in Fig. 9, all present data can be well represented by the correlation,

$$\frac{S_{T,\ c=0.5}}{S_L} = 1.74\left(\frac{u'}{S_L}\frac{P}{P_0}\right)^{0.41} \tag{4}$$

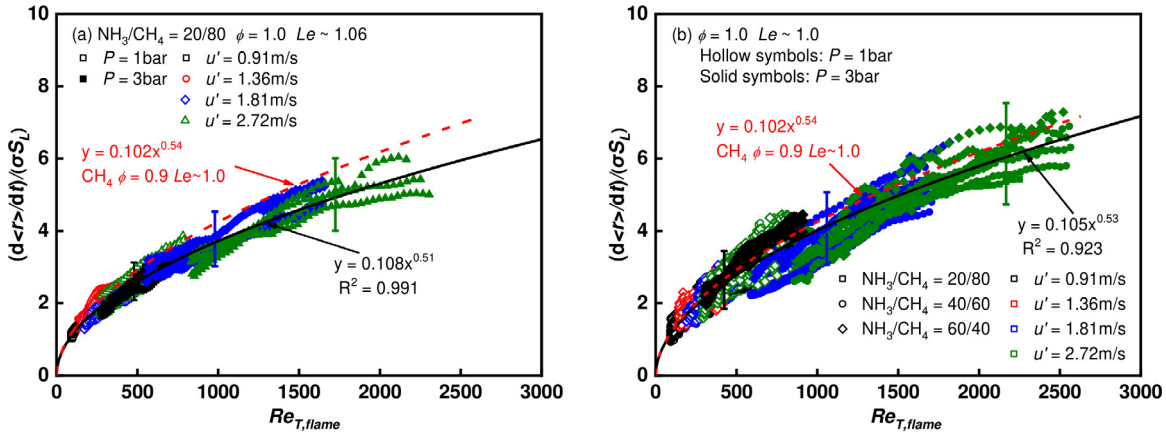

Fig. 7. Variations of normalized turbulent flame propagation speed in terms of turbulent flame Reynolds number for (a) $X_{NH3} = 0.2$ and (b) all of X_{NH3}. Previous correlation (dash red line) is plotted in comparison with present data. (For interpretation of the references to color in this figure legend, the reader is referred to the web version of this article.)

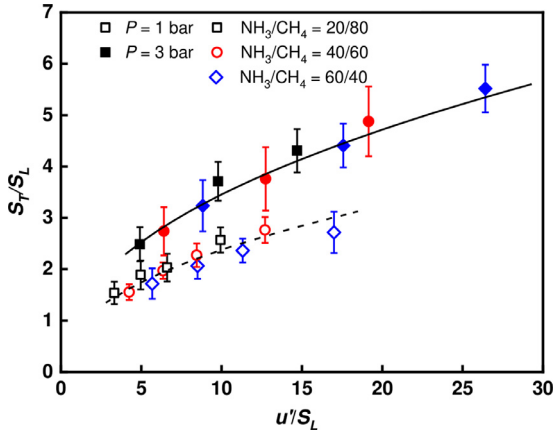

Fig. 8. Relationship between S_T/S_L with the relative turbulence intensity, u'/S_L, under different P and X_{NH3}.

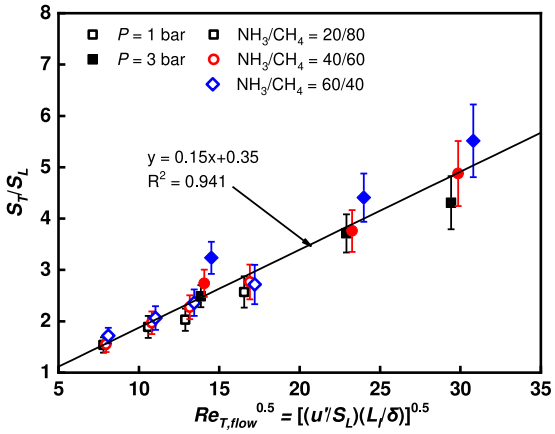

Fig. 10. Relationship between the normalized turbulent burning velocity, S_T/S_L, with the turbulent flow Reynolds number, $Re_{T,flow}$.

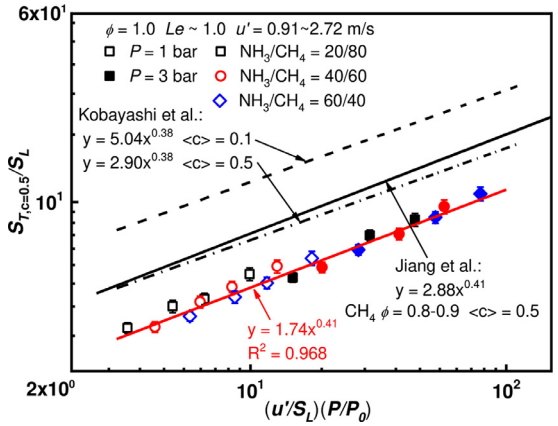

Fig. 9. The variations of $S_{T,c=0.5}/S_L$, against $(u'/S_L)(P/P_0)$. Present data are compared with previous data of turbulent Bunsen flames from Kobayashi et al. [37] and expanding flames from Jiang et al. [37].

However, compared with the correlations proposed by Kobayashi et al. [36] and Jiang et al. [37], the power exponent is almost the same, but the pre-exponent factor is quite different. Jiang et al. [37] pointed out that their experimental results at $\langle c \rangle \approx 0.5$ are different from the pre-exponent factor of Eq. (3) at $\langle c \rangle \approx 0.1$ duo to the progress variable conversion factor. Generally speaking, the S_T is the interaction result of turbulence, flame chemistry, and pressure. The effect of turbulence is usually reflected in the average fluctuation velocity of the turbulence field, that is, the turbulence intensity and the scale of turbulence eddies. Flame chemistry is usually described by S_L and δ. The effect of pressure on the flame is reflected in the decrease of S_L and δ caused by pressure increase. The largest eddies in the turbulence field is usually limited by the fan and the size of the chamber. The L_I and the largest eddies in the turbulence field are on the same order. Although the ability of the integral scale eddies maybe not enter the flame preheat zone and reaction zone, its energy is very strong, which can directly affect the flame surface. Lipatnikov et al. [63] reviewed that the effects of L_I on turbulent burning velocity may not be negligible unless $Da \gg 1$ or $Re \gg 1$. Nevertheless, Eq. (6) lacks a characterization of the turbulence length scale, which might cause the difference of pre-exponent factor between the present results and the correlation of Kobayashi et al. [36] and Jiang et al. [37]. Damköhler [35] proposed that $(S_T/S_L)^2$ is proportional to the ratio of turbulence diffusion coefficient, $D_T \sim u'L_I$, and laminar diffusivity, $D_L \sim S_L\delta$. Damköhler's correlation integrates the effects of u' and L_I, and includes the S_L and δ to consider the coupling effect of flame chemistry and pressure. This correlation is further verified by the present data, as shown in Fig. 10. According to the theoretical Damköhler's correlation, when $u'/S_L\delta$ are fixed, S_T/S_L is proportional to the turbulence integral length scale to the one-half power, $S_T/S_L \sim L_I^{0.5}$.

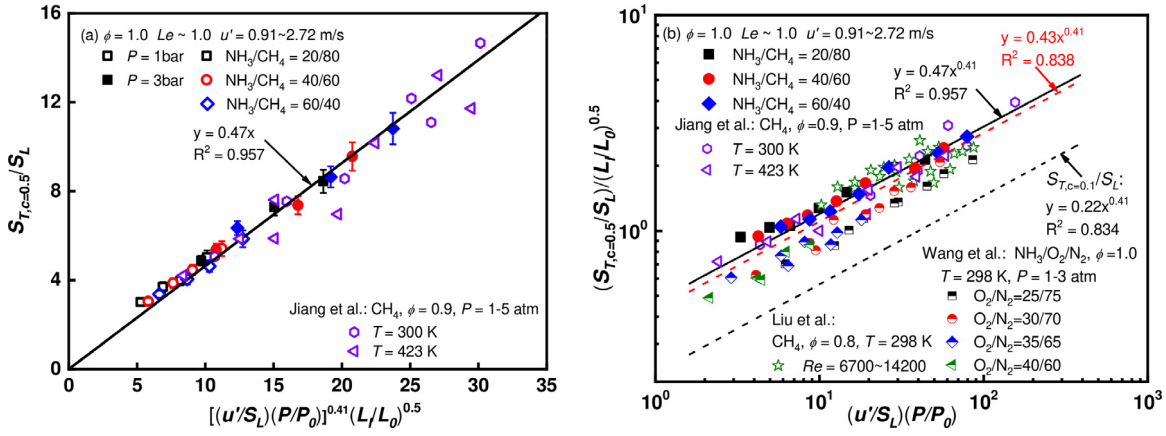

Fig. 11. (a) The modified unified correlation based on ammonia/methane/air and pure methane/air flames. (b) The variation of $(S_{T,\ c=0.5}/S_L)(L_I/L_0)^{0.5}$ with $(u'/S_L)(P/P_0)$. Literature data are from Jiang et al. [37] (CH_4/air flames), Liu et al. [31] (CH_4/air flames) and Wang et al. [30] ($NH_3/O_2/N_2$ flames).

A modified correlation is obtained by introducing an integral length scale based on the present experimental data of unity *Le* ammonia/methane/air at different X_{NH3}, *P* and *u'*:

$$\frac{S_T}{S_L} = a\left(\frac{L_I}{L_0}\right)^{0.5}\left(\frac{u'}{S_L}\frac{P}{P_0}\right)^{b} \tag{5}$$

where P_0 = 1 bar and L_0 = 1 mm for normalization. The correlation could well predict the present data and experimental data from previous spherical flames under different temperatures of Jiang et al. [37], as illustrated in Fig. 11(a). The fitting parameters *a* and *b* are 0.47 and 0.41, respectively. To further verify the applicability of this correlation, it should be compared with more hydrocarbon and ammonia fuels data measured using spherical flames from different academic groups. A large amount of experimental data of methane/air with ϕ = 0.8 over wide *Re* (6700–14,200) and the newly measured data of stoichiometric ammonia/oxygen/nitrogen turbulent expanding flames at elevated pressures (1–3 atm) are presented in Fig. 11(b). This newly modified correlation can also be successfully applied to other experimental data and can be expressed as $S_{T,\ c=0.5}/S_L = 0.43(L_I/L_0)^{0.5}[(u'/S_L)(P/P_0)]^{0.41}$ for all experimental data. All data in Fig. 11(b) converted to $\langle c \rangle \approx 0.1$ can also be good predicted by Eq. (5) with *a* = 0.22 and *b* = 0.41. It demonstrates that the present turbulent burning velocity correlation could predict the experimental data of unity *Le* ammonia fuels and pure methane flames under different pressures, temperatures and turbulence intensities.

Very recently, Lhuillier et al. [29] measured the turbulent burning velocity of ammonia/methane, ammonia/hydrogen and methane/hydrogen with ϕ = 0.9 under the same turbulence intensity. They found that the turbulent propagation characteristics of these fuels can be characterized by the *Ka* and *Da*. To further test the accuracy of the correlation for ammonia/methane/air mixtures with a higher X_{NH3}, all present experiment data is plotted in Fig. 12. The present experimental data can be well collapsed to a single line, which is represented by

$$\frac{S_T}{S_L} = 0.171 Ka^{1.01} Da \tag{6}$$

The pre-factor and power exponents of the current correlation are different from those in the literature, which may be caused by the inconsistent definition of experimental parameter, such as flame thickness. Nevertheless, this dimensionless correlation still reflects the turbulent combustion characteristics of ammonia/methane/air mixture. This correlation could be further recast as $S_T/S_L \sim Ka \cdot Da = Re_{T,\ flow}{}^{0.5}$, which is consistent with the Damköhler's correlation.

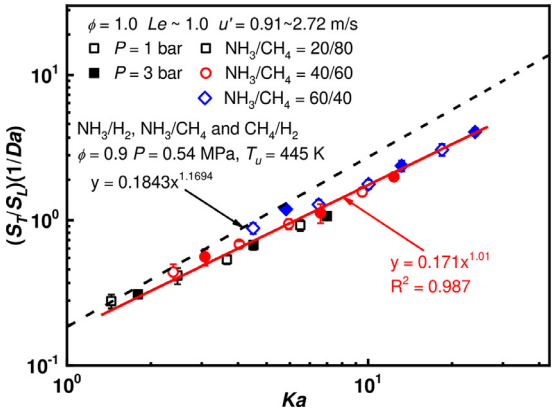

Fig. 12. The variation of $(S_T/S_L)(1/Da)$ with Karlovitz number, where *Da* is Damköhler number. The previous data line obtained based on ammonia/methane, ammonia/hydrogen and methane/hydrogen is also plotted for comparison.

Based on theoretical analysis and experimental data, the turbulent burning velocity can be characterized by $S_T/S_L \sim (L_I/L_0)^{0.5}[(u'/S_L)(P/P_0)]^{0.41}$, which shows that the turbulent burning velocity of various fuels and conditions with unity *Le* has a strong dependence on the turbulent integral scale. Liu et al. [31] proposed a fitting correlation based on the turbulent *Da*, which also considers the influence of turbulent integral scale to a certain extent. It should also be noted that the turbulence correlation discussed in this article is verified and modified based on the data of unity *Le*, and does not consider the effect of molecular transport and diffusional-thermal instability. Although Cai et al. [47] have recently developed a correlation that considers the effect of *Le* on turbulent self-similar acceleration, there is still a lack of a general turbulent combustion formula that considers the effects of turbulent integral scale and instability at the same time. Furthermore, the turbulent burning velocity definition of the common spherical expanding flame measurement method is still not uniform. Recently, Brequigny et al. [64] found that the conversion factor between different progress variables is related to the turbulence intensity. Therefore, the establishment of the correlation of turbulent burning velocity still needs to solve the above-mentioned problems.

4. Conclusions

The present work investigates the flame propagation characteristics and turbulent burning velocity of stoichiometric ammo-

nia/methane/air mixtures with the ammonia/methane molar ratio ranging from 0/100 to 60/40. The applicability of various turbulent combustion models to ammonia/methane/air flames was clarified. Then, a modified turbulent burning velocity correlation was obtained based on the data in this work and literature. The main conclusions are summarized as follows:

(1) Due to the leading role of flame chemistry, turbulent burning velocity decreases with the increase of ammonia molar content. The weakening effect of the flame chemical exceeds the enhancement of the turbulence disturbance, which causes the normalized turbulent burning velocity increase with ammonia content.
(2) The ammonia/methane/air turbulent expanding flame has the same self-similar propagation characteristics with unity Lewis number methane/air mixture regardless of ammonia content, turbulence intensity and pressure. The law of normalized turbulent burning velocity with turbulent flame Reynolds number under different ammonia molar content can be well recast to the same line, $(dr/dt)/\sigma S_L = 0.105 {Re_{T,\ flame}}^{0.53}$, which agrees well with the correlation proposed by Chaudhuri et al. [32] based on methane/air.
(3) The normalized turbulent burning velocity has obvious pressure dependence with the relative turbulence intensity. S_T/S_L scales as $(u'/S_L)(P/P_0)$ roughly to the power of 0.4, however, there is a large quantitative gap between the pre-exponential factor of the present experimental data and the turbulent burning velocities from previous work. This could attribute to the difference in the turbulence eddy scales of different experimental apparatus. A quantitative unification $S_T/S_L \sim (L_I/L_0)^{0.5}[(u'/S_L)(P/P_0)]^{0.41}$ with the consideration of the integral length scale effect is obtained. This correlation can describe not only the current experimental data but also predict the turbulent burning velocities from literature with different temperatures, pressures, and fuel types.

Declaration of Competing Interest

Authors declare that they have no conflict of interest.

Acknowledgments

This study is supported by National Natural Science Foundation of China (Nos. 52076171, 52106183), China Postdoctoral Science Foundation (No. 2021M692536). Haoran Zhao acknowledges China Scholarship Council for a joint Ph.D. scholarship at Lund University.

Supplementary materials

Supplementary material associated with this article can be found, in the online version, at doi:10.1016/j.combustflame.2022.112183.

References

[1] H. Kobayashi, A. Hayakawa, K.D.K. Somarathne, E.C. Okafor, Science and technology of ammonia combustion, Proc. Combust. Inst. 37 (2019) 109–133.
[2] C. Lhuillier, P. Brequigny, N. Lamoureux, F. Contino, C. Mounaïm-Rousselle, Experimental investigation on laminar burning velocities of ammonia/hydrogen/air mixtures at elevated temperatures, Fuel 263 (2020).
[3] A. Ichikawa, A. Hayakawa, Y. Kitagawa, K.D.K. Somarathne, T. Kudo, H. Kobayashi, Laminar burning velocity and Markstein length of ammonia/hydrogen/air premixed flames at elevated pressures, Int. J. Hydrog. Energy 40 (2015) 9570–9578.
[4] J.H. Lee, S.I. Lee, O.C. Kwon, Effects of ammonia substitution on hydrogen/air flame propagation and emissions, Int. J. Hydrog. Energy 35 (2010) 11332–11341.
[5] G.J. Gotama, A. Hayakawa, E.C. Okafor, R. Kanoshima, M. Hayashi, T. Kudo, H. Kobayashi, Measurement of the laminar burning velocity and kinetics study of the importance of the hydrogen recovery mechanism of ammonia/hydrogen/air premixed flames, Combust. Flame 236 (2022).
[6] E.C. Okafor, Y. Naito, S. Colson, A. Ichikawa, T. Kudo, A. Hayakawa, H. Kobayashi, Measurement and modelling of the laminar burning velocity of methane-ammonia-air flames at high pressures using a reduced reaction mechanism, Combust. Flame 204 (2019) 162–175.
[7] A. Ichikawa, Y. Naito, A. Hayakawa, T. Kudo, H. Kobayashi, Burning velocity and flame structure of CH4/NH3/air turbulent premixed flames at high pressure, Int. J. Hydrog. Energy 44 (2019) 6991–6999.
[8] T. Shu, Y. Xue, Z. Zhou, Z. Ren, An experimental study of laminar ammonia/methane/air premixed flames using expanding spherical flames, Fuel 290 (2021).
[9] S. Zhou, W. Yang, H. Tan, Q. An, J. Wang, H. Dai, X. Wang, X. Wang, S. Deng, Experimental and kinetic modeling study on NH_3/syngas/air and NH_3/bio-syngas/air premixed laminar flames at elevated temperature, Combust. Flame 233 (2021).
[10] C.W. Gross, S.-C. Kong, Performance characteristics of a compression-ignition engine using direct-injection ammonia–DME mixtures, Fuel 103 (2013) 1069–1079.
[11] K. Ryu, G.E. Zacharakis-Jutz, S.-C. Kong, Performance characteristics of compression-ignition engine using high concentration of ammonia mixed with dimethyl ether, Appl. Energy 113 (2014) 488–499.
[12] S. Verhelst, J.W.G. Turner, L. Sileghem, J. Vancoillie, Methanol as a fuel for internal combustion engines, Progr. Energy Combust. Sci. 70 (2019) 43–88.
[13] S.A. Shirazi, B. Abdollahipoor, B. Windom, K.F. Reardon, T.D. Foust, Effects of blending C3–C4 alcohols on motor gasoline properties and performance of spark ignition engines: a review, Fuel Process. Technol. 197 (2020).
[14] A. Valera-Medina, H. Xiao, M. Owen-Jones, W.I.F. David, P.J. Bowen, Ammonia for power, Progr. Energy Combust. Sci. 69 (2018) 63–102.
[15] C.K. Law, Combustion Physics, Cambridge University Press, 2006.
[16] O. Kurata, N. Iki, T. Matsunuma, T. Inoue, T. Tsujimura, H. Furutani, H. Kobayashi, A. Hayakawa, Performances and emission characteristics of NH_3–air and NH_3CH_4–air combustion gas-turbine power generations, Proc. Combust. Inst. 36 (2017) 3351–3359.
[17] P.F. Henshaw, T. D'Andrea, K.R.C. Mann, D.S.K. Ting, Premixed ammonia-methane-air combustion, Combust. Sci. Technol. 177 (2005) 2151–2170.
[18] U.J.P Fa Hl, M.C. Ross, J.E. Shepherd, K.O. Pasamehmetoglu, C. Unal, Flammability limits, ignition energy, and flame speeds in H_2-CH_4-NH_3-N_2O-O_2-N_2 mixtures, Combust. Flame 123 (2000).
[19] E.C. Okafor, Y. Naito, S. Colson, A. Ichikawa, T. Kudo, A. Hayakawa, H. Kobayashi, Experimental and numerical study of the laminar burning velocity of CH_4–NH_3–air premixed flames, Combust. Flame 187 (2018) 185–198.
[20] X. Han, Z. Wang, M. Costa, Z. Sun, Y. He, K. Cen, Experimental and kinetic modeling study of laminar burning velocities of NH_3/air, NH_3/H_2/air, NH_3/CO/air and NH_3/CH_4/air premixed flames, Combust. Flame 206 (2019) 214–226.
[21] Z. Tian, Y. Li, L. Zhang, P. Glarborg, F. Qi, An experimental and kinetic modeling study of premixed $NH_3/CH_4/O_2$/Ar flames at low pressure, Combust. Flame 156 (2009) 1413–1426.
[22] H. Xiao, A. Valera-Medina, P.J. Bowen, Study on premixed combustion characteristics of co-firing ammonia/methane fuels, Energy 140 (2017) 125–135.
[23] A.A. Konnov, Implementation of the NCN pathway of prompt-NO formation in the detailed reaction mechanism, Combust. Flame 156 (2009) 2093–2105.
[24] R. Ichimura, K. Hadi, N. Hashimoto, A. Hayakawa, H. Kobayashi, O. Fujita, Extinction limits of an ammonia/air flame propagating in a turbulent field, Fuel 246 (2019) 178–186.
[25] G. Hashimoto, K. Hadi, Y. Xia, A. Hamid, N. Hashimoto, A. Hayakawa, H. Kobayashi, O. Fujita, Turbulent flame propagation limits of ammonia/methane/air premixed mixture in a constant volume vessel, Proc. Combust. Inst. 38 (2021) 5171–5180.
[26] Y. Xia, G. Hashimoto, K. Hadi, N. Hashimoto, A. Hayakawa, H. Kobayashi, O. Fujita, Turbulent burning velocity of ammonia/oxygen/nitrogen premixed flame in O_2-enriched air condition, Fuel 268 (2020).
[27] K. Hadi, R. Ichimura, G. Hashimoto, Y. Xia, N. Hashimoto, O. Fujita, Effect of fuel ratio of coal on the turbulent flame speed of ammonia/coal particle cloud co-combustion at atmospheric pressure, Proc. Combust. Inst. 38 (2021) 4131–4139.
[28] Y. Xia, K. Hadi, G. Hashimoto, N. Hashimoto, O. Fujita, Effect of ammonia/oxygen/nitrogen equivalence ratio on spherical turbulent flame propagation of pulverized coal/ammonia co-combustion, Proc. Combust. Inst. 38 (2021) 4043–4052.
[29] C. Lhuillier, P. Brequigny, F. Contino, C. Mounaïm-Rousselle, Experimental investigation on ammonia combustion behavior in a spark-ignition engine by means of laminar and turbulent expanding flames, Proc. Combust. Inst. 38 (2021) 5859–5868.
[30] S. Wang, A.M. Elbaz, Z. Wang, W.L. Roberts, The effect of oxygen content on the turbulent flame speed of ammonia/oxygen/nitrogen expanding flames under elevated pressures, Combust. Flame 232 (2021).
[31] C.-C. Liu, S.S. Shy, M.-W. Peng, C.-W. Chiu, Y.-C. Dong, High-pressure burning velocities measurements for centrally-ignited premixed methane/air flames interacting with intense near-isotropic turbulence at constant Reynolds numbers, Combust. Flame 159 (2012) 2608–2619.
[32] S. Chaudhuri, F. Wu, D. Zhu, C.K. Law, Flame speed and self-similar propagation of expanding turbulent premixed flames, Phys. Rev. Lett. 108 (2012) 044503.
[33] S. Chaudhuri, F. Wu, C.K. Law, Scaling of turbulent flame speed for expanding flames with Markstein diffusion considerations, Phys. Rev. E 88 (2013) 033005.

[34] A.R. Varma, U. Ahmed, M. Klein, N. Chakraborty, Effects of turbulent length scale on the bending effect of turbulent burning velocity in premixed turbulent combustion, Combust. Flame 233 (2021).
[35] G. Damköhler, Der einfluss der turbulenz auf die flammengeschwindigkeit in gasgemischen, Ber. Bunsen. Phys. Chem. 46 (1940) 601–626.
[36] H. Kobayashi, Y. Kawabata, K. Maruta, Experimental study on general correlation of turbulent burning velocity at high pressure, Symposium (International) on Combustion 27 (1998) 941–948.
[37] H. Kobayashi, K. Seyama, H. Hagiwara, Y. Ogami, Burning velocity correlation of methane/air turbulent premixed flames at high pressure and high temperature, Proc. Combust. Inst. 30 (2005) 827–834.
[38] S.S. Shy, C.C. Liu, J.Y. Lin, L.L. Chen, A.N. Lipatnikov, S.I. Yang, Correlations of high-pressure lean methane and syngas turbulent burning velocities: effects of turbulent Reynolds, Damköhler, and Karlovitz numbers, Proc. Combust. Inst. 35 (2015) 1509–1516.
[39] L.J. Jiang, S.S. Shy, W.Y. Li, H.M. Huang, M.T. Nguyen, High-temperature, high–pressure burning velocities of expanding turbulent premixed flames and their comparison with Bunsen-type flames, Combust. Flame 172 (2016) 173–182.
[40] J. Driscoll, Turbulent premixed combustion: flamelet structure and its effect on turbulent burning velocities, Progr. Energy Combust. Sci 34 (2008) 91–134.
[41] M.T. Nguyen, D.W. Yu, S.S. Shy, General correlations of high pressure turbulent burning velocities with the consideration of Lewis number effect, Proc. Combust. Inst. 37 (2019) 2391–2398.
[42] D. Bradley, A. Lau, M. Lawes, F. Smith, Flame stretch rate as a determinant of turbulent burning velocity, Philos. Trans. R. Soc. Lond. Ser. A 338 (1992) 359–387.
[43] T. Kitagawa, T. Nakahara, K. Maruyama, K. Kado, A. Hayakawa, S. Kobayashi, Turbulent burning velocity of hydrogen–air premixed propagating flames at elevated pressures, Int. J. Hydrog. Energy 33 (2008) 5842–5849.
[44] N. Chakraborty, R.S. Cant, Effects of Lewis number on turbulent scalar transport and its modelling in turbulent premixed flames, Combust. Flame 156 (2009) 1427–1444.
[45] G. Ozel-Erol, M. Klein, N. Chakraborty, Lewis number effects on flame speed statistics in spherical turbulent premixed flames, Flow, Turbul. Combust. (2020).
[46] A.N. Lipatnikov, J. Chomiak, Molecular transport effects on turbulent flame propagation and structure, Progr. Energy Combust. Sci. 31 (2005) 1–73.
[47] X. Cai, J. Wang, Z. Bian, H. Zhao, M. Zhang, Z. Huang, Self-similar propagation and turbulent burning velocity of CH_4/H_2/air expanding flames: effect of Lewis number, Combust. Flame 212 (2020) 1–12.
[48] H. Zhao, J. Wang, X. Cai, Z. Bian, H. Dai, Z. Huang, Development of a fan-stirred constant volume combustion chamber and turbulence measurement with PIV, Front. Energy (2021) 1–15.
[49] R.J. Moffat, Describing the uncertainties in experimental results, Exp. Therm. Fluid Sci. 1 (1988) 3–17.
[50] A.J. Reiter, S.-C. Kong, Diesel engine operation using ammonia as a carbon-free fuel, Internal Combustion Engine Division Fall Technical Conference (2010), pp. 111–117. editor^editors.
[51] A.P. Kelley, C.K. Law, Nonlinear effects in the extraction of laminar flame speeds from expanding spherical flames, Combust. Flame 156 (2009) 1844–1851.
[52] X. Cai, J. Wang, H. Zhao, Y. Xie, Z. Huang, Effects of initiation radius selection and Lewis number on extraction of laminar burning velocities from spherically expanding flames, Combust. Sci. Technol. (2017) 1–26.
[53] D. Bradley, M. Lawes, M.S. Mansour, Correlation of turbulent burning velocities of ethanol–air, measured in a fan-stirred bomb up to 1.2 MPa, Combust. Flame 158 (2011) 123–138.
[54] C.K. Law, C.J. Sung, Structure, aerodynamics, and geometry of premixed flamelets, Progr. Energy Combust. Sci. 26 (2000) 459–505.
[55] N. Bouvet, F. Halter, C. Chauveau, Y. Yoon, On the effective Lewis number formulations for lean hydrogen/hydrocarbon/air mixtures, Int. J. Hydrog. Energy 38 (2013) 5949–5960.
[56] N. Peters, The turbulent burning velocity for large-scale and small-scale turbulence, J. Fluid Mech. 384 (1999) 107–132.
[57] A.W. Skiba, T.M. Wabel, C.D. Carter, S.D. Hammack, J.E. Temme, J.F. Driscoll, Premixed flames subjected to extreme levels of turbulence part I: flame structure and a new measured regime diagram, Combust. Flame 189 (2018) 407–432.
[58] S. Kheirkhah, Ö.L. Gülder, A revisit to the validity of flamelet assumptions in turbulent premixed combustion and implications for future research, Combust. Flame (2021) 111635.
[59] S. Mohammadnejad, Q. An, P. Vena, S. Yun, S. Kheirkhah, Thick reaction zones in non-flamelet turbulent premixed combustion, Combust. Flame 222 (2020) 285–304.
[60] P. Ahmed, B. Thorne, M. Lawes, S. Hochgreb, R.S. Cant, Three dimensional measurements of surface areas and burning velocities of turbulent spherical flames, Combust. Flame 233 (2021) 111586.
[61] F. Wu, A. Saha, S. Chaudhuri, C.K. Law, Propagation speeds of expanding turbulent flames of C4 to C8 n-alkanes at elevated pressures: experimental determination, fuel similarity, and stretch-affected local extinction, Proc. Combust. Inst. 35 (2015) 1501–1508.
[62] C.C. Liu, S.S. Shy, C.W. Chiu, M.W. Peng, H.J. Chung, Hydrogen/carbon monoxide syngas burning rates measurements in high-pressure quiescent and turbulent environment, Int. J. Hydrog. Energy 36 (2011) 8595–8603.
[63] A.N. Lipatnikov, J. Chomiak, Turbulent flame speed and thickness: phenomenology, evaluation, and application in multi-dimensional simulations, Progr. Energy Combust. Sci. 28 (2002) 1–74.
[64] P. Brequigny, C. Endouard, C. Mounaïm-Rousselle, F. Foucher, An experimental study on turbulent premixed expanding flames using simultaneously Schlieren and tomography techniques, Exp. Therm. Fluid Sci. 95 (2018) 11–17.